Diagnostics for liquid dispersion due to a high-speed impact with accident or vulnerability assessment application

2009 Meas. Sci. Technol. 20 025401

(http://iopscience.iop.org/0957-0233/20/2/025401)

Meas. Sci. Technol. **20** (2009) 025401 (12pp) doi:10.1088/0957-0233/20/2/025401

Diagnostics for liquid dispersion due to a high-speed impact with accident or vulnerability assessment application

Richard A Jepsen[1], Timothy O'Hern[2], Byron Demosthenous[3], Ed Bystrom[3], Mark Nissen[3], Edward Romero[3] and Sam S Yoon[4]

[1] Mechanical Environments, Sandia National Laboratories, PO Box 5800, Albuquerque, NM 87185-1135, USA
[2] Thermal, Fluid and Aero Experimental Sciences, Sandia National Laboratories, PO Box 5800, Albuquerque, NM 87185-1135, USA
[3] Applied Diagnostics, Sandia National Laboratories, PO Box 5800, Albuquerque, NM 87185-1135, USA
[4] Mechanical Engineering Department, Korea University, Anamdong, 5-Ga, Sungbukgu, Seoul, 136-713, Korea

E-mail: skyoon@korea.ac.kr

Received 18 September 2008, in final form 27 October 2008
Published 17 December 2008
Online at stacks.iop.org/MST/20/025401

Abstract
The high-speed impact and subsequent dispersion of a large liquid slug is of interest for assessing vulnerability of structures when subjected to such an event. The Weber number associated with such liquid impacts is generally between 10^5 and 10^8. Because of the experiment scale and destructive nature of these high-energy impacts, most traditional diagnostics are difficult to implement. Therefore, unique diagnostics were employed in several tests to gather information on impact force, spreading instability, slug break-up, ejection velocity, droplet deformation and spray characteristics. Measurement techniques discussed here include high-speed photometrics, particle image velocimetry (PIV), *TrackEye* particle analysis, speckle correlation, single-pass schlieren imaging, phase Doppler particle analyzer (PDPA) and load cell measurements as applied to large-scale, high-speed liquid impacts.

Keywords: impact, dispersion, vulnerability assessment, diagnostics

(Some figures in this article are in colour only in the electronic version)

1. Introduction

Sandia National Laboratories is interested in a high-speed, large liquid mass impact because of the potential for structural damage from the impact momentum transfer and subsequent thermal destruction caused by fire ignited from a splashed fuel-cloud. Here, the focus is on the liquid dispersion since it is crucial for predicting late-time thermal effects. Fire associated with large-scale liquid fuel dispersion has recently received much attention because civilian, military and government agencies are concerned about safety and reliability issues in many practical applications such as a collision of a moving vehicle with flammable storage (i.e., gas station, liquid natural gas facilities, gas/oil pipeline), or in a crash of a moving fuel tank against a structure. The dispersion characteristics of a large-scale liquid impact, which provides suitable conditions for ignition and the subsequent burning, is not well understood. This is primarily because these events have a much higher Weber number ($We = \rho D U_{\text{imp}}^2/\sigma$, where ρ, D, U_{imp}, and σ are the liquid density, drop diameter, impact speed and surface tension, respectively) than those previously tested and reported for drop impact and dispersion.

As part of a research program to investigate the high-speed, large-scale liquid impact and dispersion, several diagnostic techniques were developed and applied to visualize and measure important processes during the impact, collapse, break-up and dispersion events. Most of the tests are very destructive to the immediate surroundings resulting in

(*a*)

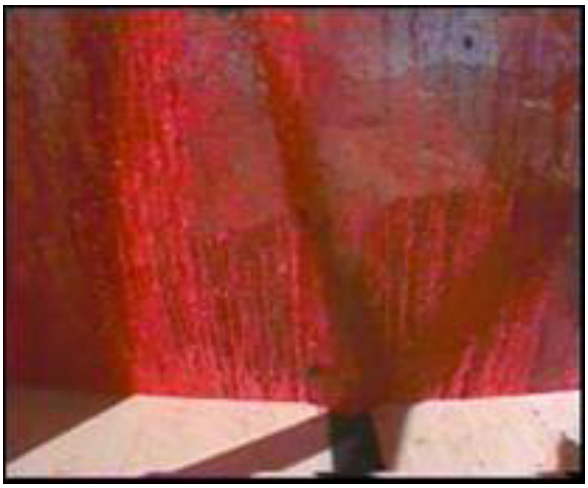

(*b*)

Figure 1. Photometric results from the water slug test. Impact velocity 105 m s^{-1} ($We \sim 10^8$): (*a*) streaks and mist cloud and fronts of the dispersion immediately following the impact; (*b*) high-speed droplets and jets of water from behind the top of the concrete structure.

limitations to the diagnostics that can be deployed near the impact event. For example, figure 1 demonstrates the scale and energy associated with one such event, in which a large tank of red dyed water impacts an unyielding wall at 105 m s^{-1} ($We \sim 10^8$). Note that the ignition of a fuel-vapor cloud, which follows the impact and dispersion of the liquid slug, will not be addressed in this paper.

While a few tests were conducted at a very high Weber number on the order of 10^8, most were done at the Weber number of 10^5 to 10^6 because of cost. Although the majority of tests were conducted at this smaller scale, they still have a relatively high Weber number as compared to previous studies [1–3]. Several diagnostic applications, some of which are unique for this test series, have been used for tests in this high Weber number regime. These include high-speed photometrics, particle image velocimetry (PIV), *TrackEye* particle analysis, speckle correlation, single-pass schlieren imaging, phase Doppler particle analyzer (PDPA) and load cell measurements. The diagnostic applications will focus on the measurement of instabilities for the spreading or splashing liquid, effects of air on spreading and splashing, and measurements during break-up and transport. Many of the aforementioned diagnostic techniques applied for such large-scale events are unique in drop impact and dispersion research. This paper describes exploratory measurements of the multiphase environment associated with very large Weber number liquid impacts on solid barriers. It is noted that the techniques have potential benefits in other fluid–solid collision applications [4–8], such as (i) cavitation damage, (ii) liquid drop impact in turbine erosion or high-speed aircraft (rain erosion), (iii) the sudden interruption of liquid flow in a pipe, (iv) cleaning or cutting materials using liquid jets, (v) wave action on sea walls and (vi) the simulation of bird strike on aircraft using liquid masses.

2. Large-scale water slug test

Tests were carried out in three scales. One test was the large water tank impact test ($We \sim 10^8$) shown in figure 1. The others were experiments done using 2–4 mm water drops and 10 cm diameter water-filled latex bladders to transport liquid slugs to the target. Here, we distinguish the definition of 'drop' from that of 'droplet'; the drop is the falling drop (whose size is relatively large) prior to impact while the droplet is the splashed droplet (whose size is relatively small) subsequent to the impact.

Very large water slug tests were performed at the 610 m sled track at the Sandia National Laboratories Validation and Qualification Sciences Experimental Complex. The tests were performed to investigate tank–wall interactions and liquid dispersion characteristics to aid in model development and validation for structural and fluid/thermal simulations of a slug impact [9]. A 1.2 m diameter aluminum cylinder (impact slug) was filled with red-dyed water. The slug was rocket propelled down the sled track to a peak velocity of about 105 m s^{-1}. The propelling rocket sled was stopped near the end of the track with a water brake, while the slug continued in motion and was allowed to fly off the end of the track for about 10 m until it impacted a concrete wall at a velocity of 105 m s^{-1}. The concrete was essentially unyielding and the slug burst upon impact. Photometrics, PIV and PDPA were the three diagnostic tools utilized for this test. The results from the applications of these individual diagnostic techniques are discussed below.

2.1. Photometrics

Digital and film cameras of 30, 100, 432 and 1000 fps captured the impact event for the large water slug impact. The wide-angle 30 fps cameras showed the radial dispersion of the water (dyed red) to distances approximately 30–40 m from the point of impact (see figure 1). The frame count indicated that it took less than 1 s for the water to reach a distance of 40 m from the impact point. Other photometric data revealed that (1) water was ejected in visible streaks and fronts as it moved radially away from the impact point. (2) Some of the water ejected from the tank traveled at high velocities out to 40 m and then the velocity immediately slowed down by two orders of magnitude due to drag. (3) The diameters of some of the ejected water droplets were on the order of millimeters to centimeters. (4) The water formed a cloud

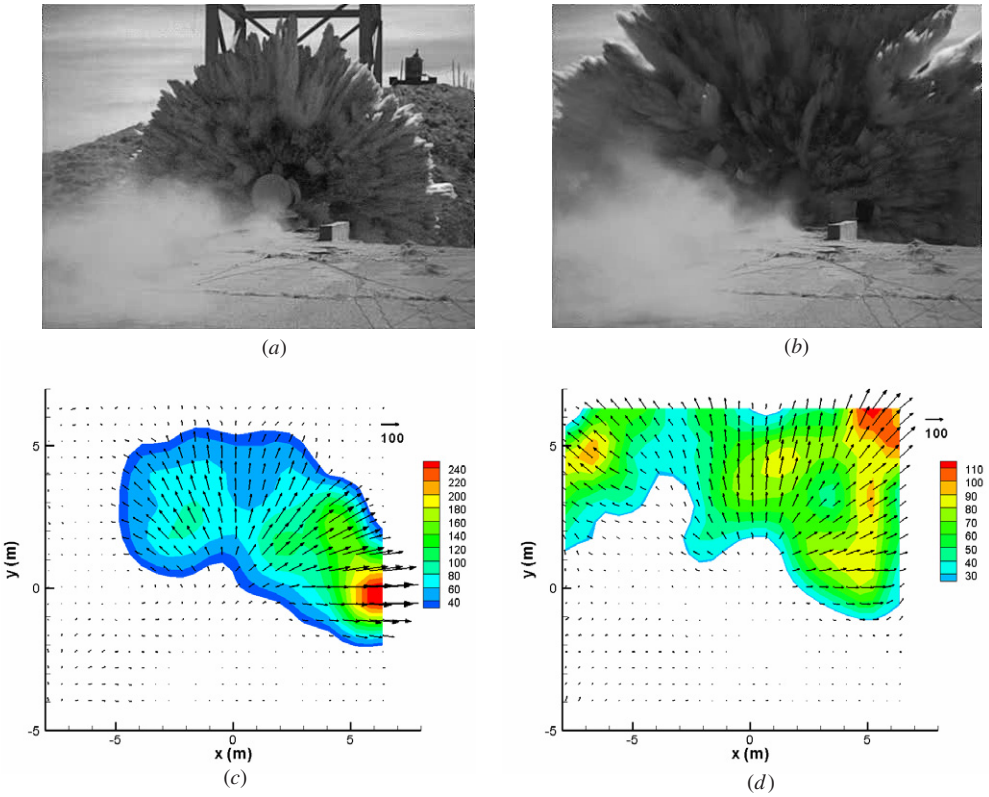

Figure 2. (*a*), (*b*) Particle images at 18 and 34 ms, respectively, after impact; (*c*) and (*d*) corresponding 2D velocity fields calculated by PIV. Velocity vectors are in m s^{-1} and positions are in m. Note different velocity ranges between (*c*) and (*d*).

of red mist that took several seconds to dissipate and settle to the ground. Furthermore, initial radial ejection velocities were slightly higher than the impact velocity, the phenomenon of which can be explained by the impact theory of Field *et al* [7]. This phenomenon was demonstrated by photometrics from a 100 fps camera, which showed the first 'ring' or 'wave' traveling at an average speed of 110 m s^{-1} over the first 10 m.

2.2. Particle image velocimetry

Particle image velocimetry (PIV) analysis was also applied to the high-speed video taken during the large water slug test [9]. The single-camera 2D PIV technique calculated the two-dimensional velocity field by the cross-correlation measurement of particle displacement between successive frames. The commercial *LaVision* PIV analysis software *DaVis* Ver. 7.2 was used. Images were captured at a sufficiently high frame rate that the displacements were relatively small (on the order of a few pixels between images). Videos at 1000 frames per second were digitized to tagged image file format (TIFF) for the analysis. Each frame was 416 × 312 pixels in size (covering a field approximately 14 by 11 m) with 8 bits per pixel gray scale. The camera was positioned off-axis from the sled motion and facing the target center. The angle between the sled track and the camera was 30°. This off-axis angle slightly affects both the symmetry and accuracy of the calculated velocities obtained from this analysis technique. Therefore, velocities on the left half of the vertical centerline of the image will be slightly over-predicted and those on the right half will be slightly under-predicted by the PIV calculations. No attempt was made to correct the PIV-measured velocity vectors for this error of ±10%.

Figure 2 shows the raw images and calculated velocity fields at 18 ms (*a*, *c*) and 34 ms (*b*, *d*) after impact. The *DaVis* settings were as follows: interrogation window size 32 × 32 pixels (approx. 1.1 m by 1.1 m), two-pass, 50% overlap. The grayscale video image in figures 2(*a*) and (*b*) provided sufficient contrast and material to be tracked to yield the velocity field vectors shown in figures 2(*c*) and (*d*). The PIV analysis yielded a maximum velocity of 250 m s^{-1} at 18 ms after impact, considerably higher than the photometric analysis value of a 110 m s^{-1} average velocity at 10 m. However, most of the velocity values were lower than this peak value and are consistent with the photometric results.

2.3. Phase Doppler particle analyzer

The phase Doppler technique is a laser Doppler velocimeter (LDV)-based method for the simultaneous measurement of single particle size and velocity (see [10] for a historical review). The fundamentals of the phase Doppler particle analyzer (PDPA) are described in [11]. The PDPA consists of a laser, transmitting optics, a receiver optics package, signal processors and data collection and analysis software, with all operations, data collection and analysis computer controlled. A phase Doppler system measures the spatial and temporal frequency of the Doppler-shifted light scattered by individual droplets or particles passing through a laser-beam-crossing

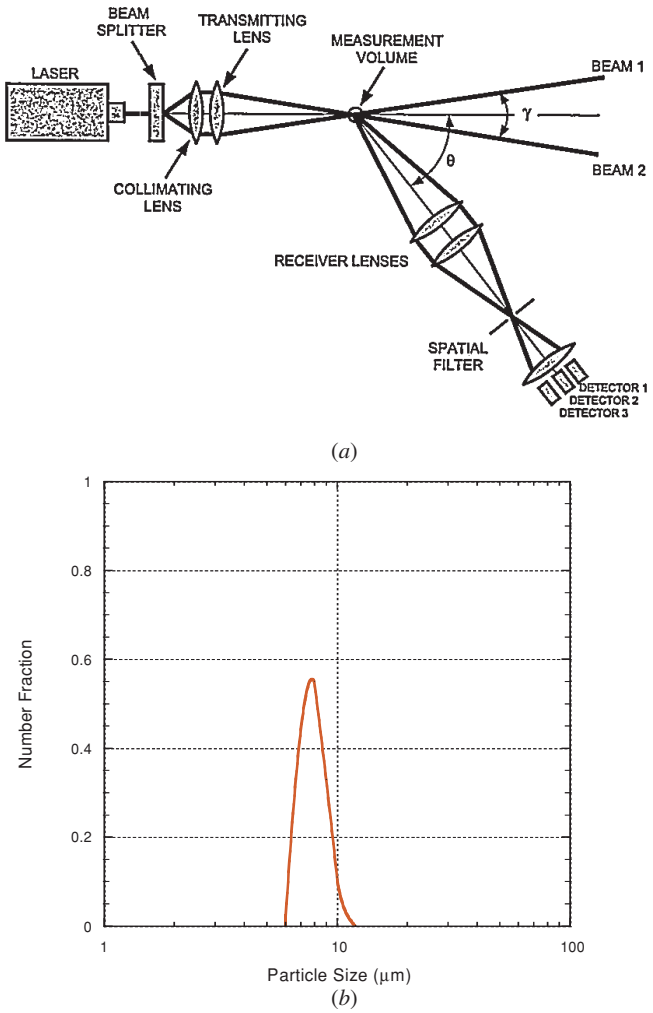

Figure 3. (*a*) Schematic of the PDPA device; (*b*) distribution of the secondarily atomized droplets, obtained from the PDPA measurement for the water slug test.

measurement volume. Phase Doppler systems use multiple photodetectors to sample slightly different spatial portions of the light scattered by individual droplets. The phase shift between two such signals is a measure of the scattered light spatial frequency, which can be directly related to the droplet diameter, refractive index and receiver geometry. Particle velocity is related to the temporal frequency in the same manner as in conventional LDV. Figure 3(*a*) is a schematic layout of a generic phase Doppler system.

Droplet sphericity is required since the phase shift is calculated for either rays refracted through spherical droplets of known, constant refractive index or reflected off the surface of reflective droplets or particles. The system used in these tests (TSI, Inc.) measures two velocity components in addition to particle size. The manufacturer-stated operating envelope includes a 0.5–10 000 m diameter range, with 1% typical accuracy and a 50:1 dynamic range, and a velocity range over 500 m s^{-1}, with 0.2% typical accuracy. This system also calculates number density based on the number of particles passing through a calculated size-dependent measurement volume (to correct for trajectory ambiguity effects). The maximum measurable number density is 10^6 cm^{-3}.

The PDPA technique was used to measure the droplet size, distribution and velocity of a small measurement volume ($\sim$1 cm^3) in the flow field approximately 20 m perpendicular from the impact point. The PDPA did not measure the transient droplet path for the test because the main water jet trajectory traveled about 0.5 m north of the sample measurement volume. This was probably due to the small deflection of the wall during the ejection of the water. However, the PDPA did measure some residual spray or mist, indicative of the final size of the droplets in the outer region. The timing sequencer cable was destroyed by flying debris during the test, so the timing was determined from the last pulse of data that was retrieved before the fiber optic cable was damaged by a large piece of debris. The results of the final particle size are shown in figure 3(*b*). As shown, the size distribution of the mist is in the range of 6–13 μm. This small size is primarily due to aerodynamically driven secondary breakup or atomization. Because the range of the gas-based Weber number, $We_g = \rho_g D U_{\text{imp}}^2 / \sigma$, is around $12 < We_g < 50$, the breakup mode is in the bag-breakup regime [12–14], in which a drop deforms/flattens and a torus-shaped ring arises at the drop's equator and eventually breaks up because of Rayleigh–Taylor instability [15–19]. In addition, evaporation may also have been present, but was less of an effect because of the short time between the dispersion event and the measurement.

3. Smaller scale water drop tests

In the smaller scale experiments, drops were introduced from a syringe injector at 2–4 mm or were delivered to the target via a spherical latex bladder for the 10 cm slugs. The Weber number for these tests was 10^3–10^6. For the 10 cm slugs, the latex was removed using a small (0.5 cm tall) blade immediately prior to impact. The latex peels away from the water in less than 1 ms, resulting in a large spherical water drop. The disturbance to the drop surface due to the quick peel-off of the latex appears to have little effect on splashing mechanisms, such as the instability-induced finger formation, since our data on finger numbers are comparable to those of previous work for a similar Weber number [1–3] (see the next section). In some tests where interactions with gas or air were measured, the latex was not removed to obtain a visually sharp leading edge of the collapsing drop.

Three main diagnostic tools (Photometrics, PDPA and load cell) were applied to the latex bladder tests. Only high-speed photometrics were applied to the 2 to 4 mm drop impact tests. Additional data were supplied through schlieren measurement and post-test PIV and *TrackEye* particle analysis.

3.1. High-speed photometrics

Much of this work required high-resolution, high-speed video for analysis to assess the collapsing, spreading, break-up and dispersion processes of liquid drops during impact. In many cases the photometric data were the basis for other diagnostic techniques and analysis. The photometric

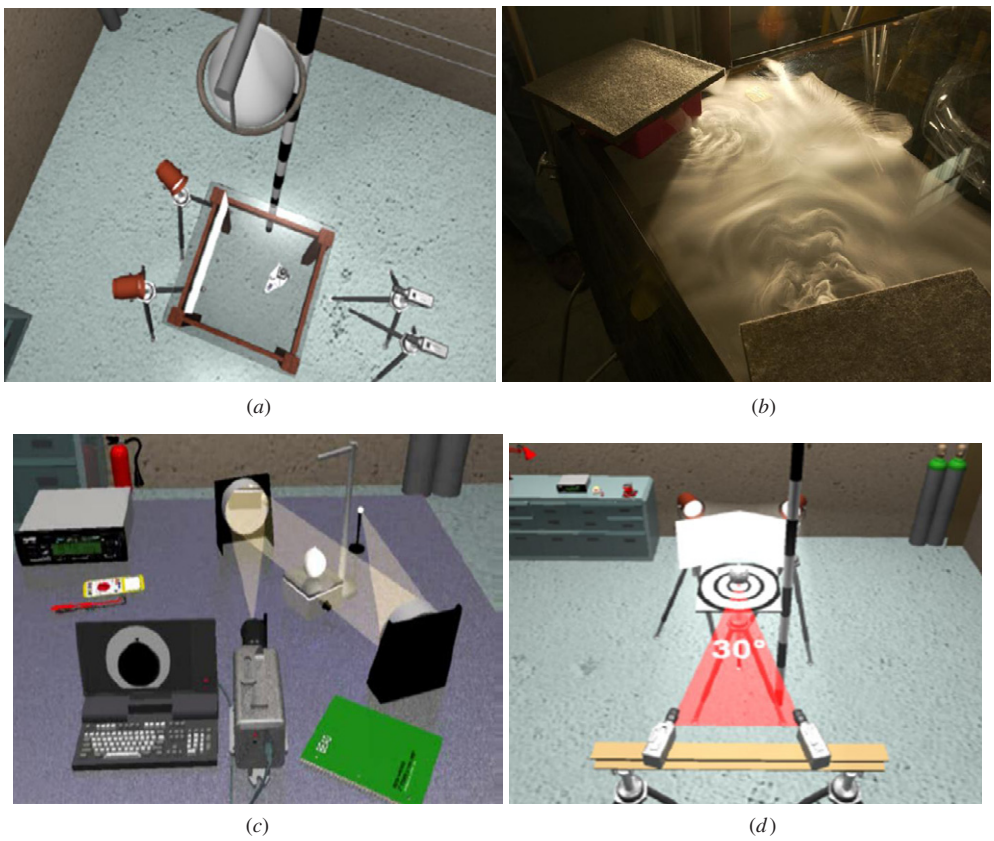

(*a*) (*b*)

(*c*) (*d*)

Figure 4. (*a*) Set-up for capturing spreading and splash on an acrylic target with three cameras (one underneath the upper-right quadrant of the clear acrylic table). (*b*) CO_2 gas cloud where the slug impacts the stable region in the upper-right corner. (*c*) schlieren set-up. (*d*) Speckle correlation set-up with two cameras.

data were gathered by using one to three digital phantom cameras (Vision Research, Wayne, NJ), arranged as shown in figures 4(*a*)–(*d*), with frame rates between 1200 and 10 000 fps and exposure times from 5 to 100 μs per frame. Both forward and backlighting techniques were used. In some cases, other visual enhancement were used, such as a thin CO_2 vapor layer in figure 4(*b*) and the schlieren method in figure 4(*c*), to observe the induced motion of the air or gas upon drop impact. Figure 4(*d*) shows the experimental set-up for speckle correlation measurements, in which two offset cameras were used for displacement measurement. Results of these photometric diagnostics will be presented in the following sections.

The limitations of the photometric techniques are primarily that optical access is needed to get high-quality images suitable for image processing and analysis. Also, the cameras must be able to acquire images fast enough to provide sufficient temporal resolution to track drop and droplet characteristics of interest.

Data were taken directly from photometrics to count the number of instabilities or fingers along the leading edge of the spreading rim; this finger counting was possible due to the sharpest visual images of the liquid–air interface with lighting applied directly underneath the PMMA (polymethylmethacrylate) target. An example of an image used for this analysis is shown in figure 5. It should be noted that the image in figure 5 is still in the transient

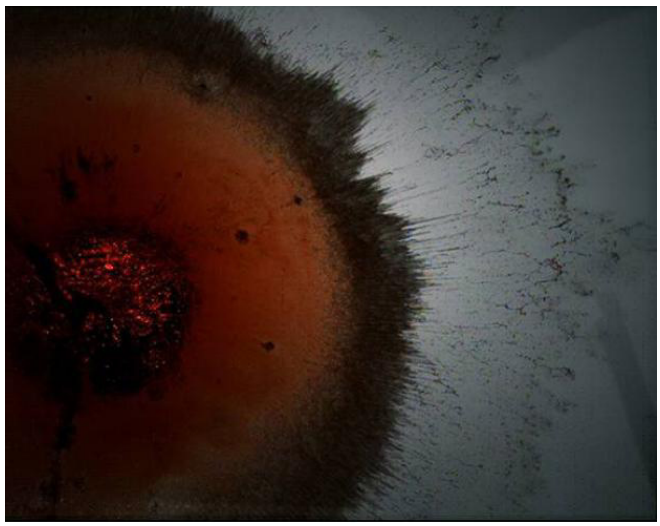

Figure 5. Fingers and splash for the large Weber number ($\sim 10^6$) impact. View is from beneath the splash surface (see figure 4(*a*)).

stage and, thereby, the local frequency of fingers along the edge seems indeterminate. However, the finger appearance becomes clearer when spreading is completed. Figure 6 plots the number of fingers ejected upon impact for a full range of test conditions: from no finger formation for $We \approx 50$ up to We of 10^9. Other data [3] were included to demonstrate their

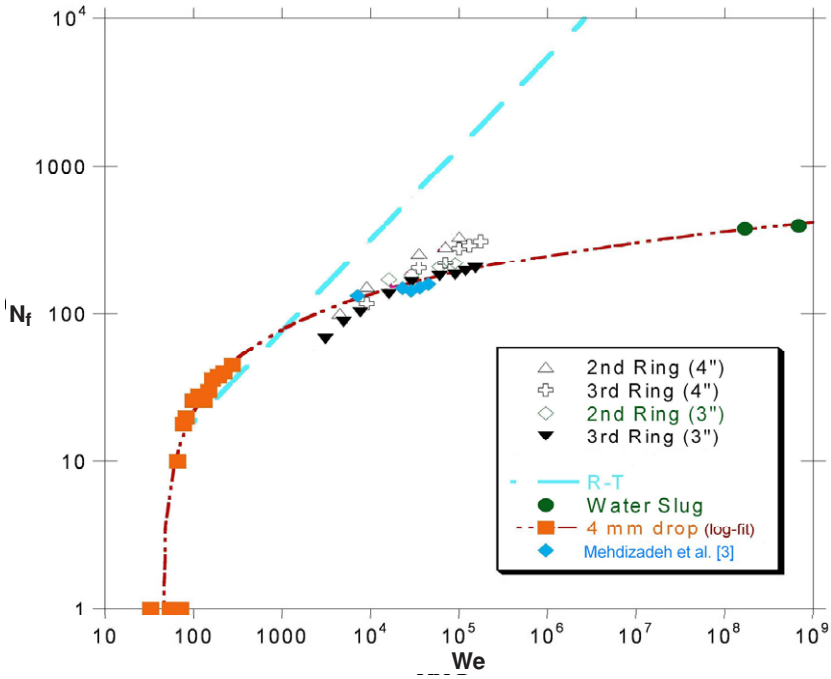

Figure 6. Number of fingers versus the Weber number for various tests. Fit through data is logarithmic.

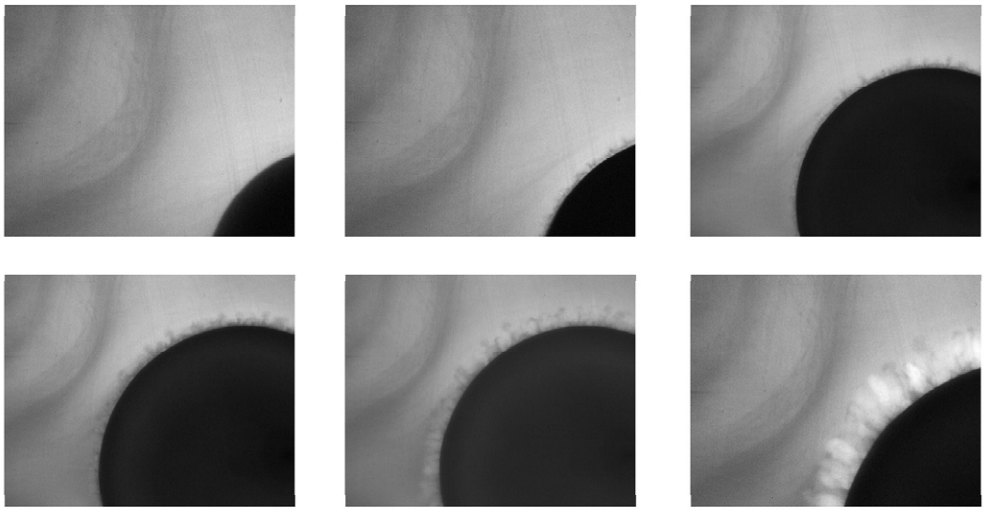

Figure 7. Time series snapshots of the finger formation of gas (CO_2) with an interval of 5 ms due to the induced azimuthal instability of air when a balloon hits the Plexiglas surface. Photos are taken beneath the Plexiglas at the bottom location.

correspondence with data collected for this work, which were collected by using different experimental techniques. Our 4 mm data agreed well with Rayleigh–Taylor theory [1–3] only for $100 < We < 300$ (intermediate Weber number), but deviated at both higher and lower Weber numbers (note the log scale). We have distinguished the second and third ring (or finger) data in figure 6; the number of fingers in the third ring is less than that of the second because finger merging occurs when the third ring overruns the second. The data for two different drop masses show that differences in the drop mass seem to result in different numbers of fingers at a constant Weber number. The difference is outside of the error tolerance and the pattern is consistent for the second and third rings. Also the empirical formula that fits the experimental data is suggested: $N_f = -92 + 57\log(We)$.

Figure 7 demonstrates the evolution of the induced motion of the air compressed and ejected during the collapsing phase of a falling drop on a thin layer of CO_2 vapor covering the target surface as shown in figure 4(*b*). The photos in figure 7 were taken from beneath the transparent PMMA. In this case, the latex on the balloon was not removed so the splash would not interfere with the air–CO_2 gas interactions. Although the balloon eventually rebounds after initial impact and collapses due to the high surface tension force of the latex, the data of interest are only for the collapsing and spreading portion of the impact. The maximum spreading of the latex-bound drop occurred at 25 ms for the event shown in figure 7.

Figure 8. Schlieren images prior to and during impact showing the compressed and displaced air (bright) ejecting from underneath the collapsing drop. Images are approximately 30 ms apart.

3.1.1. Schlieren imaging. The schlieren imaging technique was used to investigate the density gradients, due to compressibility, that occurred immediately prior to and during the impact and collapse of a 10 cm diameter latex-bound water slug. An illustration of the experimental set-up is shown in figure 4(*c*). The schlieren technique allows visualization of density gradients and movement in an otherwise transparent medium. A series of astronomical quality mirrors 60 inches apart are used to collimate a point source of light. The latex slug was made to impact a hot plate set at approximately 50 °C, which was used as a convection surface. The compressed and escaping air from the impacting and collapsing slug was observed along with vortex roll-up or primary vortical structure. Figure 8 clearly demonstrates this phenomenon with photometric data taken at 4800 fps where the escaping air appears as a jet and where the tip of the jet can be seen caught in the vortical roll-up motion. The vortical roll-up motion continues during expansion or spreading of the slug, leading to the formation of the secondary vortical structures in the azimuthal direction as shown in figure 7. These azimuthal waves of air and CO_2 gas surrounding the spreading latex slug have a similar coherent structure as that of liquid fingers. Further work needs to be done to relate the quantitative relation between liquid fingers and the azimuthal waves of CO_2 gas.

3.1.2. TrackEye particle analysis. *TrackEye* software (Image Systems AB, Sweden) was used to obtain initial splashed droplet and edge velocities from photometric data. Both private industry and military ranges use *TrackEye* for tracking and motion assessment utilizing 2D and 3D analyses. Multiple tracking algorithms allow cooperative and non-cooperative target tracking. For this analysis, a 'center of gravity' algorithm was chosen to take advantage of the image density difference between the droplets and background. Individual droplets at the end of the event were chosen and then tracked back toward the beginning of the event. The intensity parameter had to be adjusted slightly to keep track of the splashed droplets of interest as the droplet image changed in size, shape and density. Using the *TrackEye* software, the radial velocities of specific droplets or spreading edges can be determined. Figure 9 shows the results for a 5 m s^{-1} impact of a 10 cm diameter water-filled balloon for test configuration in figure 4(*a*). Randomly chosen droplets ('splash A', 'splash B' and 'splash C') were analyzed. The start time for the tracking in figure 9(*a*) was 7–27 ms after impact because the particles or spreading edge were not easily discernable at early times

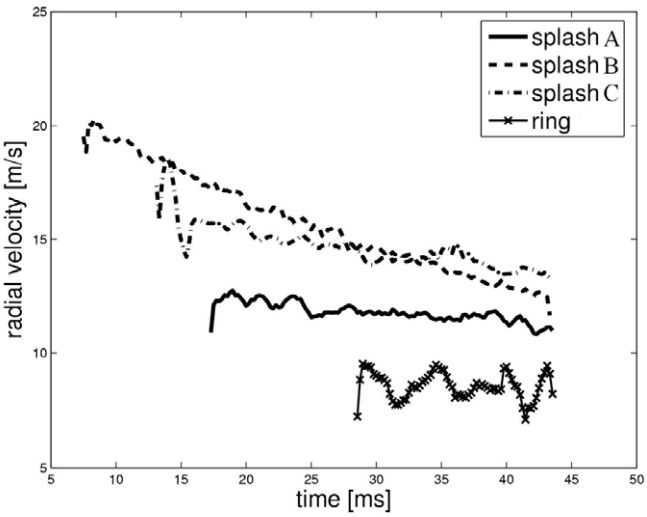

(*a*)

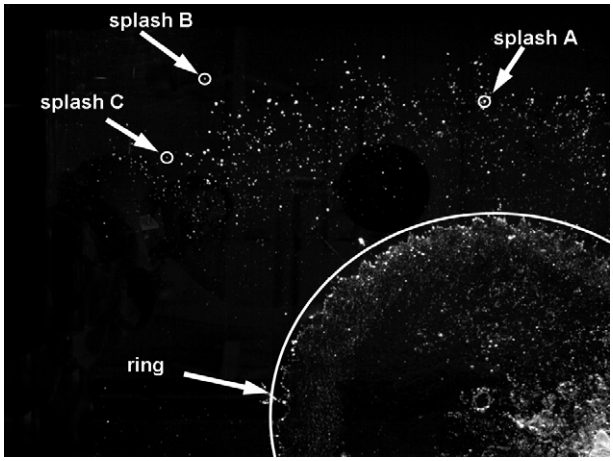

(*b*)

Figure 9. (*a*) The droplet radial velocity. The operating conditions are $U_{\text{imp}} = 5$ m s^{-1}, $D = 0.106$ m. (*b*) Image corresponding to plot (*a*) indicating where the velocity measurements were taken.

due to the interference and high density of splashing droplets. Some splashed droplets are shown to have initial velocities of four times the impact speed due to compressed air ejection and all droplets have reduced velocities with time due to drag forces.

Tests were also done with 4 mm drops impacting a variety of angled surfaces. Figure 10(*a*) shows an example of such a test. The results demonstrated that upon initial contact and

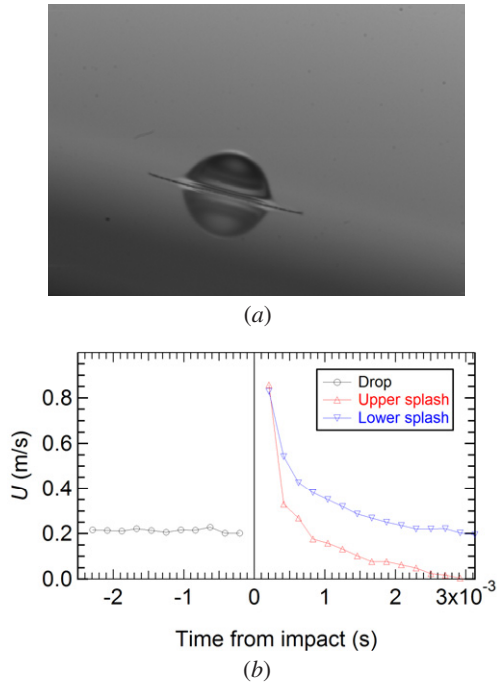

Figure 10. (*a*) A 4 mm drop impact at the 15° angle. (*b*) *TrackEye* data for the drop experiment shown in (*a*).

spreading (first data point), the 'uphill' portion of the spreading or speed was nearly equivalent to that of the 'downhill' portion (see figure 10(*b*)). However, at later time, the downhill portion of the splash maintains higher spreading velocities than the uphill portion. This difference may be due to gravity or/and the component of momentum that is tangential to the wall.

3.1.3. PIV analysis. Particle image velocimetry (PIV) analysis was also applied to video images from specific tests to investigate particle transport dynamics. PIV analysis was done for a single camera using forward and backlighting techniques from both underneath a clear acrylic table (see figure 4(*a*)) and side views of the impact and dispersion event. The backlighting was used to create particles that were 'shadows' in the image so the delineation between droplet, ligament and air could be maximized and image processing minimized. The mono-camera PIV technique allows calculation of the two-dimensional velocity field by comparing particle displacements between successive frames captured at a sufficiently high frame rate where the displacements were relatively small, on the order of a few pixels in the image. The analysis used the *LA Vision 2D PIV* and *Sizing Master* software. When forward lighting techniques were used, there was some image enhancement using a combination of image processing filters to better delineate the droplets and ligaments. This analysis provided velocity and particle size data during the break-up and splashing processes. Figure 11 shows the vector field and velocity versus particle size determined by this analysis for a 3.5 m s^{-1} impact of a 10 cm water slug recorded at 4800 fps.

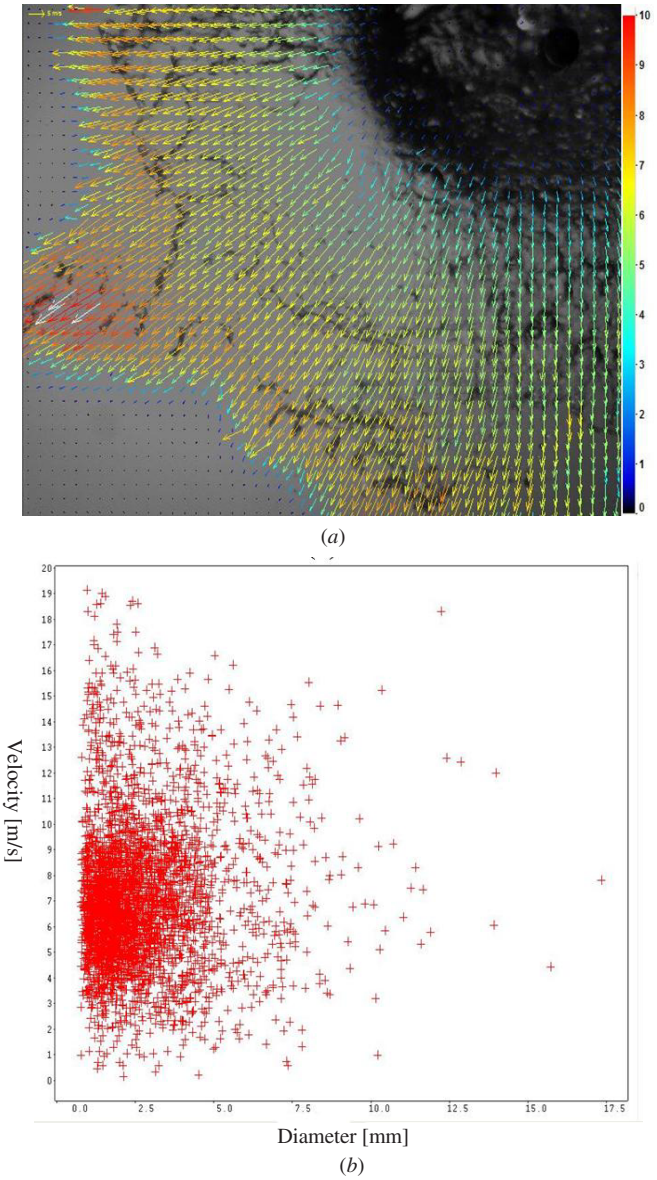

Figure 11. (*a*) Vector field for the splashing process. (*b*) Velocity from 0 to 20 m s^{-1} (*y*-axis) versus the particle size diameter from 0 to 18 mm (*x*-axis) during break-up and dispersion.

3.2. Speckle correlation

The speckle correlation technique [20] was used to investigate the traveling capillary waves or ripples that occur within a few millisecond during the impact of a drop of low Weber number as shown in figure 12(*a*). This phenomenon is seen for small drops on the order of millimeters or less [21]. In order to simulate this phenomenon on a larger scale, a latex-bound water slug was used to simulate a high surface tension and thus a low Weber number. This simulation is similar to that of a small water drop at low impact speed. This test also allows for the surface of the slug or latex to be covered with a high density of random dots or speckles applied by a permanent marker. Speckle correlation utilizes two calibrated, synchronized cameras to analyze the velocity, displacement and strain characteristics of an object in three dimensions. Advanced software designed by *Correlated Solutions* tracks a

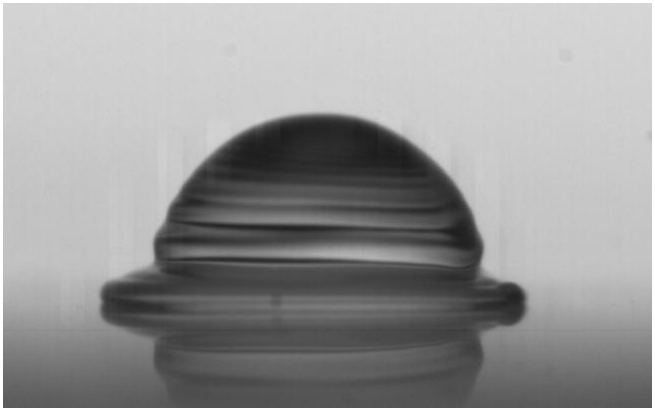

(*a*)

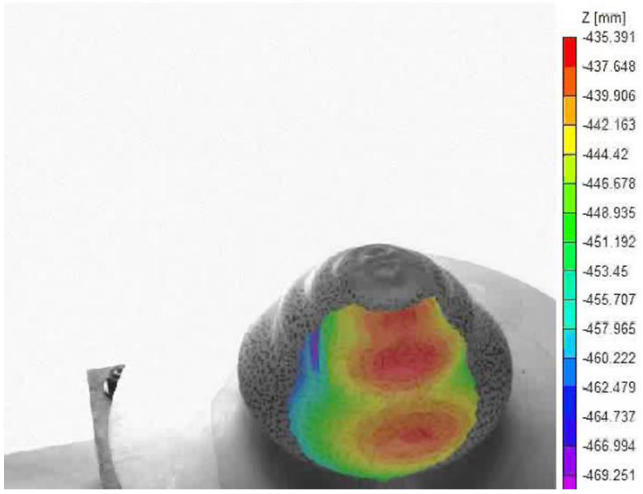

(*b*)

Figure 12. (*a*) Impact of a 4 mm water droplet at $We = 100$. (*b*) Speckle correlation for the impact of a 10 cm latex-bound water slug at the impact speed of 5 m s^{-1}.

field of closely spaced, random, high-contrast speckles on the surface of the subject. This tracking, which is done by examining a user-selected area of interest in the speckle field, determines the relationship between the speckles from one frame to the next. An illustration of the test set-up is shown in figure 4(*d*). Figure 12(*b*) shows an example of the results for an impact test of a 10 cm latex-bound water slug impacting at 2 m s^{-1}. The contours on the figure provide displacement information, and the data are recorded with sufficient time resolution to obtain the wave speed and frequency. This technique captured both high-frequency capillary waves during initial impact and low frequency waves from recoil and rebound.

3.3. Phase Doppler particle analyzer (PDPA)

The PDPA system can measure individual droplet size and velocity for each droplet passing through a small measurement volume in the flow field. This technique was used to investigate the dispersed spray created from high impact speeds and subsequent splashing. A schematic of the PDPA is shown in figure 3(*a*). The spray was collimated through a 1 cm

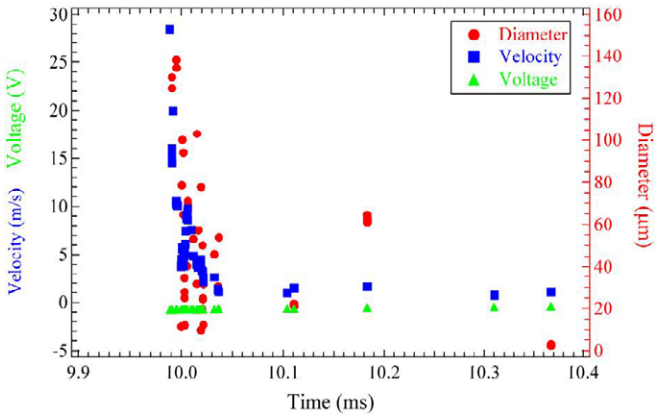

Figure 13. PDPA results for splash at a 36 cm radius from impact and 2.5 cm above the impact surface. The external voltage input was used for timing with a load cell at impact. From this timing fiducial, impact occurred at 9.98 s.

wide 3 cm high slot so the PDPA equipment would not get wet during testing. An external voltage input was used in the PDPA measurements for synchronizing time zero with a load cell upon impact. Results of a high-speed, large slug impact test ($We \sim 10^6$) are shown in figure 13. This figure shows that the expanding droplet front after impact has the fastest moving, largest particles, which were ejected during the splash. Subsequent droplets slow down and are smaller than those in front.

PDPA was also used for the very large Weber number impacts of 10^8. In this case, the PDPA measurement system was housed in a steel bunker approximately 60 ft (18 m) to one side of the impact point. A small, collimated window allowed for spray to enter the sample volume without harming the equipment due to flying debris or fluid. Although the placement of the sample volume missed the transient jet of spray ejected from the impact point, it did measure the residual spray as it drifted and settled to the ground (see section 2.3).

3.4. Impact force measurements

Impact force tests were done to gain insight on the force-time history during the impact and spreading of a liquid slug. These tests were conducted using 10 cm diameter water slugs. The water slug impacted the load cell assembly shown in figure 14, which comprised a 30 cm diameter target plate, an internal force sensor, a 4 cm long blade to remove the latex centered on the target plate and a 60 kg reaction mass. In some cases, the latex was removed using the blade technique and in other cases it was left intact. The target plate absorbed and transferred the impact force of the water slug to the internal force sensor.

Data were recorded using a *Hi-Techniques WIN600* high-speed data acquisition system. The data were sampled at 1 MHz with no filter and the total sampling time was 1 s including 250 ms of pre-trigger data. The force sensor signal from the load cell assembly and a burst signal were the two channels of data collected for each test. An Inter Range Instrumentation Group (IRIG-B) time code signal was used

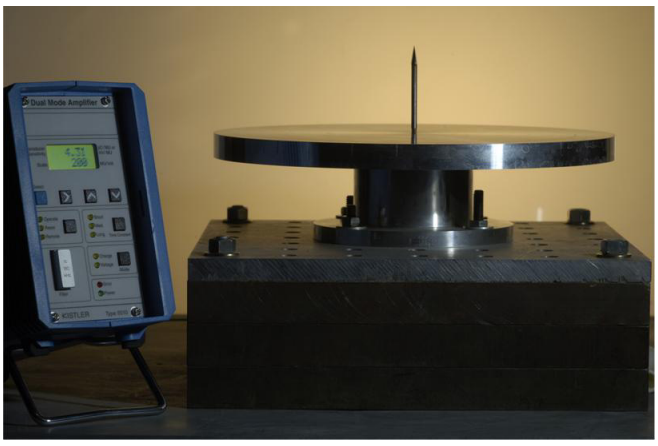

(*a*)

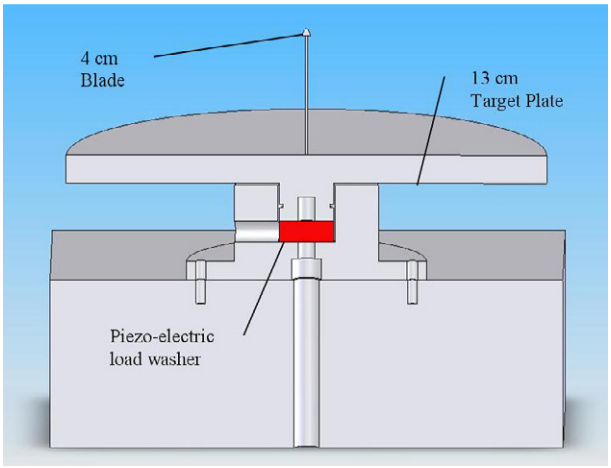

(*b*)

Figure 14. (*a*) Load cell and target assembly with an amplifier. (*b*) Cross-sectional schematic of the load cell.

as the time-base for the WIN600. The system was triggered at impact by using a threshold of 20 percent full-scale force.

The IRIG-B and burst signal were used to assure synchronization between data collection systems: the *WIN600*, *Phantom* high-speed digital cameras and PDPA. The ±1 V burst signal was supplied from an *Agilent 33120 A* waveform generator and recorded on both the *WIN600* and particle analyzer. The IRIG-B time-base signal was supplied from a *True Time A20-501-000* GPS receiver and recorded on both the *WIN600* and high-speed digital cameras.

The internal force sensor in the load cell assembly was a *Kistler 9031A* quartz piezoelectric load washer. The *Kistler 9031A* is designed to measure dynamic and quasi-static forces between 0 and 60 KN. The load cell was mounted between the target plate and 60 kg reaction mass as shown in figure 14(*b*). The charge output from the load washer was converted to voltage with a *Kistler 5010B* dual mode charge amplifier and a 180-kHz low-pass filter. An amplifier sensitivity of 4.31 pC N^{-1} and an output of 100–200 N V^{-1} were used.

The data were analyzed using Sandia National Laboratories developed *K2 v.9* data analysis software. Fast Fourier transforms (FFTs) of the force data consistently

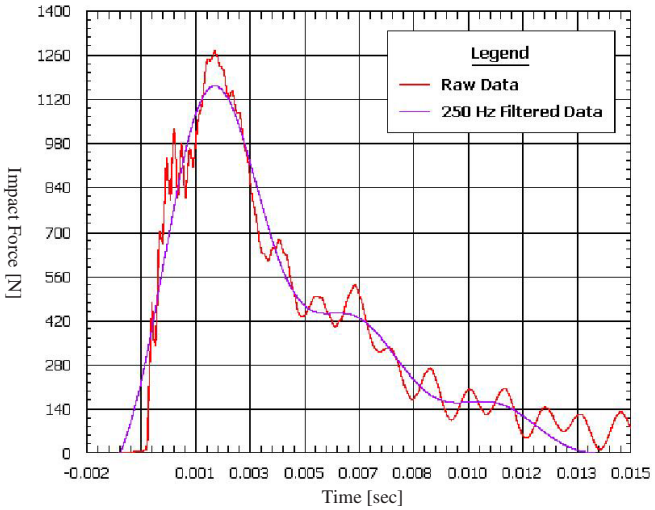

Figure 15. Load cell data for a 10 cm diameter water slug impacting at 10.8 m s^{-1}.

indicated that the majority of the energy content for water slug impacts was below 250 Hz. Small excursions were observed at ∼500 and ∼850 Hz, likely corresponding to the natural frequencies of various components of the experimental hardware. Force data were filtered using a 250 Hz low-pass 6-pole Butterworth, and forward filtering and backward filtering were performed to eliminate time shifts.

A typical example of load cell data from a water slug impacting at 10.8 m s^{-1} is shown in figure 15. In this case, the latex was removed and the water slug collapsed and spread unimpeded by the latex. The data show an initial impact pulse with peak force of 1297 N at 2.8 ms, a second pulse at 6.5 ms and a third pulse at 11 ms. The pulses cannot be associated with the natural frequency of the plate since they are not symmetric and are much lower (<300 Hz) than the 700 Hz natural frequency of the load cell assembly. An extremely high initial pressure in the liquid–solid contact periphery, namely 'compressed region', presumably exists according to Field *et al* [7]; $P = \rho C U_{\text{imp}}$, where C is the shock wave velocity in the liquid.

Corresponding data from photometrics show the visual effects of the pulsing measured by the load cell which manifests itself in distinct spreading *fronts* and multiple *waves* (or *rings*) induced from pressure bouncing (or pulsation) within the collapsing liquid. Figure 16 shows the time series snapshots of the impacting slug for the load cell data shown in figure 15. At about 3 ms, the centerline of the slug or maximum diameter impacts the plate. This coincides with the peak force measured by the load cell at 2.8 ms after the initial impact. Between about 6 and 7 ms, a bulge on the top of the impacting slug can be seen, and it begins to increase its vertical motion beyond 7 ms. This pulse coincides with the load cell data where the second pulse occurs at about 6.5 ms. It is difficult to visualize any other pulses from this view, and the smaller third pulse from the load cell data is not observable from the photometrics.

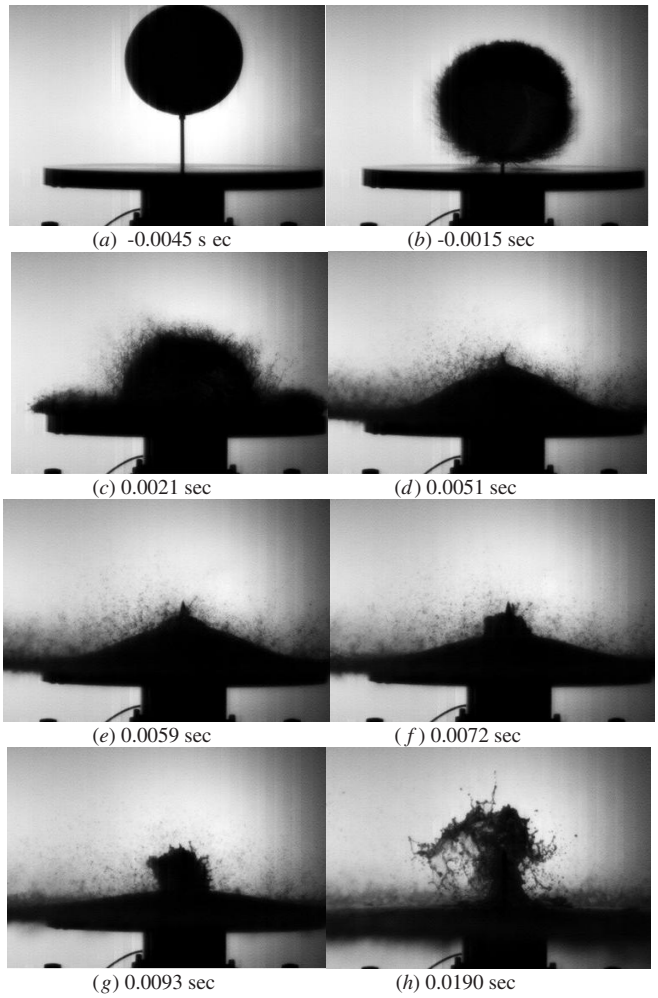

Figure 16. Photometric data for a 0.6 kg water slug impacting at 10.8 m s^{-1} for the load cell plot shown in figure 15. Timing coordinated with the load cell plot of figure 15.

4. Conclusion

The investigation of large liquid slug impact, break-up and dispersion has led to the development of several new diagnostics. The basis for most of the acquired data was high-speed photometrics and image processing. Photometrics supported diagnostics such as particle image velocimetry (PIV), *TrackEye*, schlieren, speckle correlation and impact force measurements. The direct data obtained through photometrics included the finger instability of the splashed liquid and the development of compressed CO_2 motion during the collapse of a falling drop. The schlieren imaging technique was particularly aimed at the visualization of the vortex roll-up motion of air just prior to and during drop collapse at impact. The *TrackEye* and PIV analysis provided the velocities of the splashed droplets and the spreading rate of the remaining liquid. The speckle correlation technique was used to investigate the traveling capillary waves or ripples along the surface of the impacted liquid of pyramidal shape. Finally, a load cell or force plate assembly measured the impact force of the falling bladder in which three prominent pulsations were measured. Much of the testing described here has been done for high Weber number impact events in which destructive energy is present and traditional diagnostics are difficult to employ. All of the techniques utilized for these tests have successfully provided essential data and new insights on the liquid impact, break-up and dispersion process.

Acknowledgments

Sandia is a multiprogram laboratory operated by Sandia National Lab (SNL), a Lockheed Martin Company, for the United States Department of Energy's National Nuclear Security Administration under contract DE-AC04-94AL85000. The corresponding author acknowledges that part of this research was supported by the Korea Science and Engineering Foundation (KOSEF) grant funded by the Korea government (MEST), no R11-2007-028-03001.

References

[1] Allen R F 1975 The role of surface tension in splashing *J. Colloid Interface Sci.* **51** 350–1
[2] Aziz S D and Chandra S 2000 Impact, recoil and splashing of molten metal droplets *Int. J. Heat Mass Transfer* **43** 2841–57
[3] Mehdizadeh N Z, Chandra S and Mostaghimi J 2004 Formation of fingers around the edges of a drop hitting a metal plate with high velocity *J. Fluid Mech.* **510** 353–73
[4] Lesser M B 1981 Analytic solutions of liquid drop impact problems *Proc. R. Soc.* A **377** 289–308
[5] Lesser M B and Field J E 1983 The impact of compressible liquids *Ann. Rev. Fluid Mech.* **15** 97–132
[6] Field J E, Lesser M B and Dear J P 1985 Studies of 3-d liquid wedge impact and their relevance to liquid-drop impact problems *Proc. R. Soc.* A **401** 225–49
[7] Field J E, Dear J P and Ogren J E 1989 The effects of target compliance on liquid drop impact *J. Appl. Phys.* **65** 2–10
[8] Field J E 1999 Liquid impact; theory and applications *Wear* **233** 1–12
[9] Jepsen R A, Jensen K and O'Hern T J 2004 Water dispersion modeling and diagnostics for water slug impact test *SEM Conf. (Irvine, CA, June)*
[10] Hirleman E D 1996 History of development of the phase-Doppler particle-sizing velocimeter *Part. Part. Syst. Charact.* **13** 59–67
[11] Bachalo W D and Houser M J 1984 Phase Doppler spray analyzer for simultaneous measurements of drop size and velocity distributions *Opt. Eng.* **23** 583–90
[12] Pilch M and Erdman C 1987 Use of break-up time data and velocity history data to predict the maximum size of stable fragments for acceleration-induced break-up of a liquid drop *Int. J. Multiph. Flow* **13** 741–57
[13] Lee C S and Reitz R D 2001 Effect of liquid properties on the breakup mechanism of high-speed liquid drops *Atomization and Sprays* **11** 1–19
[14] Joseph D D, Belanger J and Beavers G S 1999 Breakup of a liquid drop suddenly exposed to a high-speed airstream *Int. J. Multiphase Flow* **25** 1263–303
[15] Joseph D D, Beavers G S and Funada T 2002 Rayleigh-Taylor instability of viscoelastic drops at high Weber numbers *J. Fluid Mech.* **453** 109–32
[16] Varga C M, Lasheras J C and Hopfinger E J 2003 Initial breakup of a small-diameter liquid jet by a high-speed gas stream *J. Fluid Mech.* **497** 405–34
[17] Joseph D D 2005 Motion of a spherical liquid drop in a high-speed airstream *Int. J. Multiphase Flow* **31** 1059–62

[18] Zeoli N and Gu S 2006 Numerical modeling of droplet break-up for gas atomization *Comput. Mater. Sci.* **38** 282–92

[19] Aliseda A, Hopfinger E J, Lasheras J C, Kremer D M, Berchielli A and Connolly E K 2008 Atomization of viscous and non-Newtonian liquids by a coaxial, high-speed gas jet. Experiments and droplet size modeling *Int. J. Multiphase Flow* **34** 161–75

[20] Hild F and Roux S 2006 Digital image correlation: from displacement measurement to identification of elastic properties—a review *Strain* **42** 69–80

[21] Renardy Y, Popinet S, Duchemin L, Renardy M, Zaleski S, Josserand C, Drumright-Clarke M A, Richard D, Clanet C and Quere D 2003 Pyramidal and toroidal water drops after impact on a solid surface *J. Fluid Mech.* **484** 69–83